The effect of chimney entrance slope and constricted section on the performance of solar chimney power plants: a CFD approach

Mahmut Kaplan[1*]

[1]Gaziantep University, 27600 Gaziantep, Turkey

Abstract. The depletion of hydrocarbon resources and climate change are major global issues which need to be solved urgently. Sun is a clean, inexhaustible, sustainable energy source which has the capacity to meet the future energy demands. Solar chimney power plants (SCPPs) with a simple design are competent to generate large-scale electricity. Primary components of SCPP are the chimney, turbine, and collector. In this work, impact of the chimney entrance slope and narrowed section on performance of SCPP is scrutinized. A computational fluid dynamics model (CFD) is constructed based on Manzanares plant with a chimney height (H) of 194.6 m via ANSYS FLUENT. The novel configurations are generated by changing the chimney inlet slope, θ (45°-85°) and radius of the constricted section with a fixed height (H/28). The findings demonstrate that a decrease in the slope with the constricted section improves the velocity, power and turbine pressure drop. The highest velocity of 17.9 m/s is gained for the configuration with θ = 85° compared to that of 14.3 m/s obtained for the base (θ = 45°) at 1000 W/m^2. This configuration enhances power output to 60.4 kW with a rise of 31.3% in comparison to the base case at 1000 W/m^2.

1 Introduction

Fossil fuels are finite resources that have a profound impact on air pollution and climate change. Therefore, renewables like wind, solar, hydropower, biomass and geothermal play a key role in decarbonizing power production. Among them, the sun offers free and clean energy in abundance. Solar chimney power plants (SCPPs) have the technical competence to meet the large-scale sustainable power generation. SC utilizes the solar thermal energy to produce electricity according to the fundamental principles of physics. They comprise three main parts: the collector, turbine and chimney. Hot air needed to the chimney is provided by the greenhouse phenomenon under the collector. Its roof is enveloped by a transparent layer which is located at a distance from the floor.

Ambient air entering from the bottom of the plant is heated through a transparent canopy on account of the greenhouse effect. Since the warmed air underneath the collector is lighter than the cold air in the chimney, the upward air motion driven by buoyancy force

* Corresponding author: mahmutkaplan@gantep.edu.tr

is induced throughout the tower. The flow of energy contained in the updraft operates turbine located close to chimney entrance and thus mechanical energy obtained by the air is transformed into electricity employing a generator. Under the collector, various high-energy storage density materials such as visqueen, canvas, gravel, ceramic and concrete are employed to produce uninterrupted power through night and cloudy-sky day. Heat stored by these materials during daytime is discharged from the absorber surface after sunset or cloudy days to produce continuous power [1].

Performance of SCPP system is affected by geometric shapes of solar chimney components such as ground, collector and chimney. Modification of primary dimensions such as the radius, height and slope of the chimney and collector has a significant impact on the efficiency of the SC system. Aziz and Elsayed [2] computationally examined the influence of chimney angle (0°-5°) and inlet height from the ground on the SC performance. They reported that changing chimney angles and inlet heights considerably impacted the system efficiency and the optimum angle was determined as 3°. Ali et al. [3] accomplished computational fluid dynamics (CFD) simulation based on geometrical characteristics of the Manzanares prototype to scrutinize the influence of distinct dimensions of the plant components, ambient temperatures and solar radiation on power output via MATLAB-Simulink environment. The findings demonstrated that the radius of the collector had a great influence on temperature variation compared to the chimney height and air temperature is in direct proportion with the electricity generated from the solar chimney plant. They also suggested new equations to predict the optimum collector radius.

Kaplan [4] improved innovative SCPP configurations with inclination angles ranging from 50° to 80° via ANSYS FLUENT. It was seen that an increase in the angle of inclination augmented the flow and turbine pressure drop features near the chimney entrance. The peak velocity and power output values were obtained with 80° inclination angle. Djimli et al. [5] conducted an experimental and numerical study to evaluate the influence of chimney outlet radius (4-18 m) on the efficiency of SCPP. They noticed that a rise in the radius of chimney outlet by nearly two times inlet radius led to the significantly improvement of the SC overall efficiency in comparison to other configurations. Mandal et al. [6] improved a SC model on the basis of ANSYS FLUENT software to optimize the Manzanares prototype dimensions including the collector inlet height (0.1-1.85 m), inlet diameter (10.16-55.88 m) and outlet diameter (10.16-38.48 m) of the chimney. Their results illustrated that the power of 117.42 kW (2.3 times more than the reference case) was gained with 0.2 m collector inlet height. Besides, an increase in the chimney outlet by keeping the height fixed resulted in further increase in the power of SCPP at the expense of higher implementation costs.

Based upon present state of art regarding SC, it has been noticed that the basic geometrical features of the distinct system components including the radius, height, divergent and convergent angles are studied too much. In spite of the wide-ranging research works carried out on flow parameters, power generation and efficiency of SCPPs, the parameters about modified solar chimney geometries and their effects of the system's performance are still incomplete and not detailed in the literature. Motivation from the previous investigations provides some limited results related to the chimney entrance and therefore, in this work, effect of the chimney inlet geometry on the SCPP performance is examined.

The goals of the study are to establish new chimney entrance configurations to enhance flow features and power generation of the plant and provide more insights and new perspectives for the design of SCPP. The findings will be useful for researchers, designers, and engineers focusing on building new design methods to develop more effective and cost-efficient plants.

2 Numerical procedure

In this work, 3D geometries and meshes are created utilizing ANSYS Meshing and Design Modeler. Figure 1 displays boundary conditions and the tetrahedral mesh generated for the model.

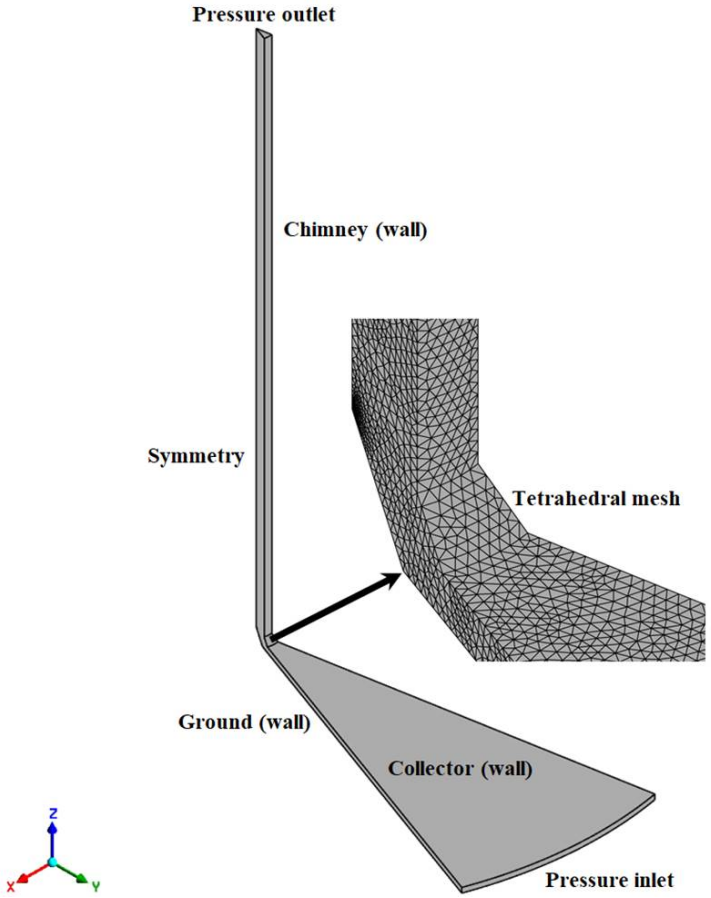

Fig. 1. Schematic of the model with boundary conditions and the mesh.

As seen in Figure 1, the computational domain is limited to 30° part of SCPP model to the reduce computation time. Collector height and radius are 1.85 m and 122 m. Chimney radius (R) and height (H) are 5.08 m and 194.6 m [7]. The chimney, collector and ground thicknesses are 0.00125, 0.004 and 0.5 m [8]. It is assumed that the air flow is incompressible, steady-state and three-dimensional. Thermo-physical characteristics are considered as independent of temperature.

The boundary conditions implemented for distinct faces of SC components are shown in Figure 1. The adiabatic, opaque and semi-transparent walls are selected for the chimney, ground and collector surfaces, respectively. The pressure inlet and outlet conditions are set for the collector inlet and chimney outlet. 0 Pa pressure and an ambient temperature of 293.15 K are chosen for the inlet and outlet. Heat flux (q) of 0 W/m^2 is specified to the chimney. The convection thermal condition is assigned at the roof and heat transfer coefficient (h) is 10 W/m^{2}K [9]. A 30° portion of the computational domain is considered to lessen the iteration period. Thus symmetry condition is defined to the surfaces as illustrated in Figure 1.

Table 1 demonstrates the material features of the SCPP parts.

Table 1. Material characteristics employed for the simulations [10].

Property	Ground	Collector	Chimney
Thermal conductivity (W/mK)	1.8	1.2	202
Density (kg/m^3)	2160	2500	2719
Specific heat (J/kgK)	710	750	871
Refractive index	1	1.516	1
Transmissivity	-	0.9	-
Emissivity	0.9	0.9	1
Absorption coefficient	0.9	0.03	0

The governing equations in the cylindrical coordinate are given in Table 2.

Table 2. Governing equations used in the CFD model [11].

Governing equations	Mathematical expressions
Continuity	$\frac{1}{r}\frac{\partial}{\partial z}(r\rho u)+\frac{\partial}{\partial z}(\rho w)=0$
Momentum	$\frac{1}{r}\frac{\partial}{\partial r}(\rho uu)+\frac{\partial}{\partial z}(\rho Vw)=-\frac{\partial p}{\partial r}+\frac{1}{r}\frac{\partial}{\partial r}\left(\mu r\frac{\partial}{\partial r}(u)\right)+\frac{\partial}{\partial z}\left(\mu\frac{\partial}{\partial z}(u)\right)-2\mu\left(\frac{u}{r^2}\right)$ $\frac{1}{r}\frac{\partial}{\partial r}(\rho uw)+\frac{\partial}{\partial z}(\rho Vw)=-\frac{\partial p}{\partial z}+\frac{1}{r}\frac{\partial}{\partial r}\left(\mu r\frac{\partial}{\partial r}(w)\right)+\frac{\partial}{\partial z}\left(\mu\frac{\partial}{\partial z}(w)\right)-(\rho_0-\rho)g$
Energy	$\frac{1}{r}\frac{\partial}{\partial r}(r\rho uT)+\frac{\partial}{\partial z}(\rho VT)=\frac{1}{r}\frac{\partial}{\partial r}\left(r\frac{\lambda}{c_p}\frac{\partial}{\partial r}(T)\right)+\frac{\partial}{\partial z}\left(\frac{\lambda}{c_p}\frac{\partial}{\partial z}(T)\right)$

In this study, the air density, ρ is evaluated employing Boussinesq approximation owing to negligible density change in the SC [12].

$$(\rho-\rho_a)g\approx-(T-T_a)\rho_a\beta \quad (1)$$

where T_a and ρ_a are the ambient temperature and density. ρ_a = 1.205 kg/m^3. g is the gravitational acceleration and β is thermal expansion coefficient. A dimensionless quantity, Rayleigh number (Ra) is employed to calculate the natural convection.

$$Ra=\frac{g\beta\Delta TH_c^{\,3}}{\nu\alpha} \quad (2)$$

where H_c is the of the collector height. ΔT is the change in air temperature. ν and α are

the kinematic viscosity and thermal diffusivity. The turbulent flow in the SCPP is estimated using RNG *k*-*ε* model. The turbulent kinetic energy (*k*) and dissipation rate (*ε*) equations are

$$\frac{\partial}{\partial x_i}\left(\rho k u_i\right)+\frac{\partial}{\partial t}\left(\rho k\right)=\frac{\partial}{\partial x_j}\left(\mu_{eff}\alpha_k\frac{\partial k}{\partial x_j}\right)-Y_M-\rho\varepsilon+G_b+G_k+S_k \tag{3}$$

$$\frac{\partial}{\partial x_i}\left(\rho\varepsilon u_i\right)+\frac{\partial}{\partial t}\left(\varepsilon\rho\right)=\frac{\partial}{\partial x_j}\left(\mu_{eff}\alpha_\varepsilon\frac{\partial \varepsilon}{\partial x_j}\right)+C_{1\varepsilon}\frac{\varepsilon}{k}\left(C_{3\varepsilon}G_b+G_k\right)-C_{2\varepsilon}\rho\frac{\varepsilon^2}{k}-R_\varepsilon+S_\varepsilon \tag{4}$$

The discrete ordinates (DO) radiation and solar ray tracing models are employed to predict radiative heat transfer because it is suitable for semi-transparent walls [13].

$$\nabla.\left(I\left(\vec{r},\vec{s}\right)\vec{s}\right)+\left(\sigma_s+a\right)I\left(\vec{r},\vec{s}\right)=\frac{\sigma_s}{4\pi}\int_0^{4\pi}I\left(\vec{r},\vec{s}'\right)\phi\left(\vec{s}.\vec{s}'\right)d\Omega'+an^2\frac{\sigma T^4}{\pi} \tag{5}$$

where I is the solar intensity. $\vec{s}$, $\vec{s}'$ and $\vec{r}$ are the direction, scattering and position vectors. Ω', ϕ and n are the solid angle, phase function and refractive index. σ_s and a represent scattering and absorption coefficients. To simulate the solar load on the semi-transparent collector, the ray tracing algorithm is utilized. The irradiation and solar beam direction for the position, date and time specified according to Manzanares condition are calculated employing the solar calculator. Longitude and latitude are 3.37° west and 38.99° north, respectively. The air mass flow rate $\left(\dot{m}\right)$ is

$$\dot{m}=\rho Q \tag{6}$$

where Q is the volumetric flow rate. The turbine pressure drop, Δp_t is evaluated by means of the following equation:

$$\Delta p_t=r_t p_t \tag{7}$$

where r_t represents the ratio of turbine pressure drop and r_t = 2/3 [9]. In Equation (7), the turbine pressure drop, p_t is found using the simulation findings. It is taken into account that the turbine is situated 9 meters above the base [9]. Power output, P_o is calculated from [14]

$$P_o=\eta_t Q\Delta P_t \tag{8}$$

where η_t is the efficiency of a turbine and η_t = 0.8 [15]. The FLUENT code is utilized to solve the basic transport equations coupled with turbulence and DO radiation models. In current work, SIMPLE algorithm is utilized to solve equations. The problem is regarded to be solved for all variables when the difference between two successive iterations is lower than 10^{-4}.

The innovative configurations in Figure 2 contain constricted sections with slope of 45°-85°. Height of constricted sections is fixed as *H*/28 (6.95 m) due to the location of the Manzanares SCPP turbine (9 m above the ground).

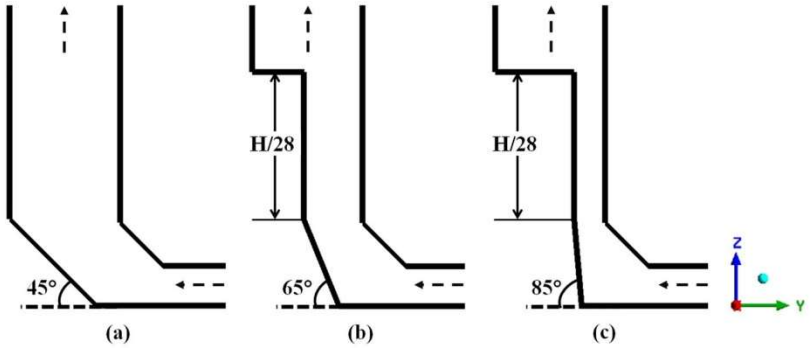

Fig. 2. Configurations: (a) base (45°), (b) 65° and (c) 85°.

3 Results and discussion

In this study, a CFD simulation is accomplished to examine the impacts of new chimney configurations with distinct slopes on the flow and performance characteristics of the SC.

The cell number of 812442 is utilized for all calculations. To verify CFD model, the findings are compared with the experimental [16] and numerical results [10, 15, 17, 18] for solar radiation (G) of 800-1000 W/m^2 in Figure 3.

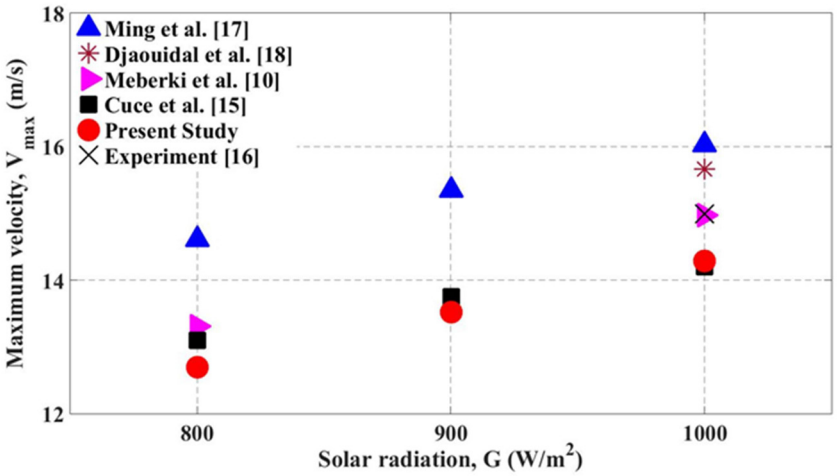

Fig. 3. Comparison of present work with existing experimental and computational studies.

It is seen in Figure 3 that the estimated maximum velocity (V_{max}) values gained in the current study is good agreement with experiment [16] in comparison to the prior computational results [10, 15, 17, 18] for 800 and 1000 W/m^2. The highest error between values is 6% at 800 W/m^2. The results are also in consistency with the estimated results obtained by Meberki et al. [10] and Cuce et al. [15] at 800-1000 W/m^2.

The calculated results for the maximum velocity, air mass flow rate, turbine pressure drop and power output obtained from base and novel configurations at 1000 W/m^2 are illustrated in Table 3.

Table 3. Comparison of the findings for base and new configurations at 1000 W/m^2.

Configurations	V_{max} (m/s)	$\dot{m}$ (kg/s)	Δp (Pa)	P_o (kW)
Base (45°)	14.3	1018.6	102.0	46.0
65°	15.8	979.3	124.2	53.9
85°	17.9	754.0	181.1	60.4

As illustrated in Table 3, increasing chimney entrance slope with a decrease in the chimney constricted section radius leads to a noticeable increase in the peak velocity, turbine pressure drop and power output of SC but at the cost of lower mass flow rate compared to the base model. The peak turbine pressure drop of 181.1 Pa and lowest mass flow rate of 754.0 kg/s are gained with the configuration having the slope of 85° as seen in Table 3. The highest power output of 60.4 kW is noticed with the chimney entrance having a 85 degree slope. This configuration enhances the power output by 31.3% in comparison the base. It is seen that alteration of geometry near the chimney base augmented SC performance as reported Aziz and Elsayed [19] and Kaplan [4].

Figure 4 demonstrates the pressure distribution of chimney entrance and narrowed sections for configurations with distinct slopes of 45° (base), 65° and 85° at 1000 W/m^2.

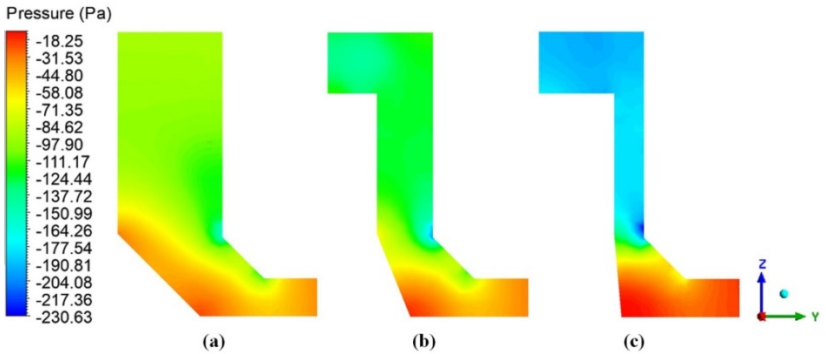

Fig. 4. Pressure distribution of different configurations: (a) 45° (base), (b) 65°and (c) 85° at 1000 W/m^2.

It is apparent in Figure 4 that non-uniformity and negative pressure increases with a higher slope and smaller radius of narrowed chimney section compared to base configuration. But an increase in the slope and a decrease in the section radius lead to reduced chimney entrance area. This limits access of air to the chimney in Figures 4(b) and (c). Therefore, a 26% reduction in mass flow rate is examined for the configuration with the slope of 85° at 1000 W/m^2 compared to the base case.

Through comparing the CFD results, it is found that the turbine pressure drop is of great significant in the design of the SCPPs and enhancement of the power output as shown in Equation 8. Further decrease in chimney section area results in much lower mass flow rate and problems related the real-world applicability of SC.

4 Conclusions

In this paper, a 3D CFD investigation is carried out to examine the impacts of innovative chimney entrance configuration with distinct slopes (45°-85°) and constricted sections on

flow and performance characteristics utilizing ANSYS FLUENT software. The primary findings are summarized as follows:

- Modification of chimney entrance slope and the constricted section close the chimney inlet influences air mass flow rate, turbine pressure drop and thus the power output.
- A rise in chimney entrance slope with narrowed chimney section results in considerable enhancement in negative pressure near the turbine. This augments SC power output as illustrated in Equation (8).
- The peak velocity of 17.9 m/s and the peak power output of 60.4 kW are achieved with the slope of 85°. This configuration augments the power output by 31.3% in comparison with the base at 1000 W/m^2.
- The configuration with 85° slope decreases investment costs by reducing dimensions of chimney entrance compared to the base case.
- The constricted chimney section height and size of chimney entrance area should be limited to improve turbine efficiency and avoid detrimental effects on air flow features.

References

1. E. Cuce, P. M. Cuce, S. Carlucci, H. Sen, K. Sudhakar, M. Hasanuzzaman, R. Daneshazarian, Sustainability **14**, 1450 (2022)
2. A. Aziz, A. M. Elsayed, Renew. Energ. **200**, 674–693(2022)
3. M. H. Ali, Z. Kurjak, J. Beke, Int. J. Thermofluids **20**, 100434 (2023)
4. M. Kaplan, Int. J. Photoenergy **2023**, 7394007 (2023)
5. S. Djimli, T. E. Boukelia, A. Chaker, A. Ghellab, Environ. Prog. Sustain. Energy **43**, e14275 (2024).
6. D. K. Mandal, N. Biswas, N. K. Manna, D. K. Gayen, A. C. Benim, Sci. Rep. **14**, 979 (2024)
7. W. Haaf, K. Friedrich, G. Mayr, J. Schlaich, Int. J. Sol. Energy **2**, 3–20 (1983)
8. E. Cuce, P. M. Cuce, H. Sen, K. Sudhakar, U. Berardi, U. Serencam, Int. J. Photoenergy, **2021**, 6612222 (2021)
9. E. Cuce, A. Saxena, P. M. Cuce, H. Sen, S. Guo, K. Sudhakar, Int. J. Low Carbon Technol. **16**, 704–714 (2021)
10. A. Mebarki, A. Sekhri, A. Assassi, A. Hanafi A, B. Marir, Energy Rep. **8**, 500–513 (2022)
11. H. Nasraoui, Z. Driss, H. Kchaou, J. Therm. Anal. Calorim. **140,** 2721–2732 (2020)
12. D. K. Mandal, N. Biswas, N. K. Manna, A. C. Benim, Ain Shams Eng. J. **15,** 102390 (2024)
13. S. R. Keshari, C. V.P., P. Das, Sol. Energy, **226**, 455–467 (2021)
14. Kaplan M., Engineering. Technology Quarterly Reviews, **6,** 39-48 (2023)
15. E. Cuce, H. Sen, P. M. Cuce, Sustain. Energy Technol. Assess. **39**, 100704 (2020)
16. R. Rabehi, A. Chaker, Z. Aouachria, M. Tingzhen, Int. J. Green Energy **14**, 971–982 (2017)
17. T. Ming, W. Liu, G. Xu, Int. J. Energy Res. **30**, 861–873 (2006)
18. B. Djaouida, Z. Aouachria, A. H. Benmachiche, S. Ali, Int. J. Ambient Energy, **41**, 1467–1481 (2020)